Geomechanics and Engineering, *Vol. 19, No. 3 (2019) 241-254*
DOI: https://doi.org/10.12989/gae.2019.19.3.241

Three-dimensional finite element modelling and dynamic response analysis of track-embankment-ground system subjected to high-speed train moving loads

Qiang Fu[a] and Yang Wu*

School of Civil Engineering, Guangzhou University, Guangzhou Higher Education Mega Center, 230 Wai Huan Xi Road, Guangzhou 510006, P.R. China

(Received August 8, 2019, Revised October 16, 2019, Accepted October 19, 2019)

Abstract. A finite element approach is presented to examine ground vibration characteristics under various moving loads in a homogeneous half-space. Four loading modes including single load, double load, four-load, and twenty-load were simulated in a finite element analysis to observe their influence on ground vibrations. Four load moving speeds of 60, 80, 100, and 120 m/s were adopted to investigate the influence of train speed to the ground vibrations. The results demonstrated that the loading mode in a finite element analysis is reliable for train-induced vibration simulations. Additionally, a three-dimensional finite element model (3D FEM) was developed to investigate the dynamic responses of a track-ballast-embankment-ground system subjected to moving loads induced by high-speed trains. Results showed that vibration attenuations and breaks exist in the simulated wave fronts transiting through different medium materials. These tendencies are a result of the difference in the Rayleigh wave speeds of the medium materials relative to the speed of the moving train. The vibration waves induced by train loading were greatly influenced by the weakening effect of sloping surfaces on the ballast and embankment. Moreover, these tendencies were significant when the vibration waves are at medium and high frequency levels. The vibration waves reflected by the sloping surface were trapped and dissipated within the track-ballast-embankment-ground system. Thus, the vibration amplitude outside the embankment was significantly reduced.

Keywords: track-embankment-ground system; vibration response; finite element model; moving train load; fast Fourier transform

1. Introduction

In recent years, with the rapid development of high-speed railway, the studies on the dynamic response of ground and environmental vibration induced by moving trains have attracted attention. The movement of the track structure (rail, sleeper, embankment ballast, and ground) generates stress waves that propagate into the surrounding soil when the trains pass by. Recent technological advances have created new possibilities for ground vibrations analysis. Accordingly, it is now possible to predict and reduce the vibration levels. The track structure response induced by a moving train depends on several factors including the wheel axles spacing, axle weight, and train speed. The periodic vibration frequency of the train is determined by its geometry, while other frequencies originating from the sleeper spacing are also essential.

The steady-state vibration of a periodically supported beam on an elastic half-space under a uniformly moving harmonic load has been studied by Metrikine and Popp (1999). Krylov's model was valid when the train speed was close to the critical phase velocity of the coupled track-soil system. Sheng *et al*. (2003), Lombaert *et al*. (2006), Auersch (2008) and Saeed Cheshmehkani *et al*. (2016) noticed that the quasi-static excitation was dominant. Lefeuve-Mesgouez *et al*. (2002), Lefeuve-Mesgouez and Mesgouez (2008), and Yao *et al*. (2016) had conducted this investigation using analytical means in a homogeneous elastic half-space or by semi-analytical models for multi-layered ground. Lefeuve-Mesgouez (2002) theoretically investigated the transmission of vibrations over the ground surface, and the vertical harmonic rectangular loads. The interior of the ground was modelled as an elastic half-space. Sun *et al*. (2010) and Cai *et al*. (2008) employed an analytical approach to investigate dynamic responses of a track system and the poroelastic half-space soil medium subjected to a moving point load in a three-dimensional space.

Restrictions are often imposed on the geometry and material properties of the research objective for a given analytical approach. This is because the closed-form solutions cannot be easily obtained for most practical situations. Madshus and Kaynia (2000), Bian *et al*. (2015), Bian *et al*. (2016) presented a dynamic analysis model comprising of track, embankment, layered ground, analyzing ground vibrations generated by high-speed trains moving at a critical speed. Cai and Raymond (1994) considered the interaction between the railway track and the underlying soil. The rail track was idealized as a periodic elastically coupled beam system resting on a Winkler foundation. The moving loads were applied on the railway

*Corresponding author, Associate Professor
E-mail: yangwuuu0226@hotmail.com
[a]Ph.D.
E-mail: fuqutdhhu@163.com

ISSN: 2005-307X (Print), 2092-6219 (Online)

track to investigate the dynamic response of the railway track and soils. Kouroussis *et al*. (2009) and Kouroussis *et al*. (2011) assumed that the soil could be reasonably decoupled from the track. This approach initially considered the train/track subsystem. Subsequently, the simulated ground forces were applied on a finite/infinite element model of a soil subsystem. The infinite elements were placed on the border of the mesh to properly represent an unbounded domain.

Li *et al*. (2018) established a finite element model of a ballasted railway with an infinite boundary considering the effects of moving train loads and Rayleigh waves. The proposed model was successfully validated against the results of Euler-Bernoulli Elastic Beam (E-BEB) model. Chong *et al*. (2017) presented a finite element simulation method to investigate the feasibility of detecting unfavorable substructure conditions using a moving train load. The train load module was developed by converting the train load into time-variant equivalent forces. The moving forces based on the shape functions were applied at the nodes. Hino *et al*. (1984), Shih *et al*. (2016), and Ren *et al*. (2019) presented a moving load model to analyze the propagation and attenuation characteristics of the vibration in soft soil or other mediums.

With the rapid development of high-performance computers, numerical simulations emerge as an effective tool for wave propagation and geo-structure deformation prediction in geotechnical engineering (Zhang *et al*. (2018), Chen *et al*. (2019a), Chen *et al*. (2019b), Goh *et al*. (2019)). Based on the combination of the boundary element method (BEM) and the finite element method (FEM), numerical analyses of railway-induced ground vibrations have also been examined by several authors. Sheng *et al*. (2006), Yaseri *et al*. (2014), Correia dos Santos *et al*. (2017) and Kece *et al.* (2019) used a FEM/BEM approach for the analysis of ground vibration induced by trains. Galvin *et al*. (2007a) and Galvin *et al*. (2007b) presented a general three-dimensional model for soil motion analysis and the effect of high-speed train passage on nearby surface and underground structures. A general and fully three-dimensional multi-body-finite element-boundary element model was presented by Galvin *et al*. (2010). The model was formulated in the time domain to predict vibrations due to the train passage on the vehicle, track, and free field. Both quasi-static and dynamic excitation mechanisms originating from train passage were considered. Based on the boundary element method, Kouroussis *et al*. (2014) presented a full three-dimensional FEA for the prediction of railway ground-borne vibrations. Infinite elements at the model boundary were also used.

Kaynia *et al*. (2000), Takemia *et al*. (2005) have conducted research works on the vibrations of railway, embankment, and viscoelastic half space ground (Cui *et al*. (2018)). The system was divided into several formulated substructures. Simulation functions were performed to identify vibrations of the system. Both the boundary element method and radiation damping were considered. Hall (2003) and Ju *et al.* (2010) used the finite element method to perform 3D time-domain simulation for train-induced vibrations of embankment on layered ground. However, irregularities in geometry and materials of the structure and underlying soils, which maybe encountered in practice, cannot be simply dealt with.

Absorbing boundaries were used to simulate the infinite boundary condition of ground. An implicit solver was employed for step-by-step time integration of the dynamic equilibrium equations. Hall (2003) considered the railway structure in three-dimensional models. The moving point loads were applied on the nodes in the beam elements simulating the rail. The beam elements were Bernoulli–Euler type and were given the geometry condition and properties of regular railway rails (UIC 60). The rail was connected to the sleeper by sharing nodes at the surface of sleepers. However, the dynamic response of the railway track was lacking in the finite simulation.

In this study, a numerical analysis approach was established to simulate the ground vibrations induced by high-speed trains passing through the ground surface and validate the reliability of this proposed simulation method in a homogeneous elastic half-space layer. The ground vibration response in a viscoelastic half-space subjected to different moving load modes with dynamic components was investigated. Three different dynamic boundaries including fixed boundary (FIX), infinite boundary (INF), and infinite with damping boundary (DINF) were considered, to verify the dynamic absorption efficiency of damping and the infinite elements. Moving train loads were applied on the rails represented by 8-noded solid elements. Finally, the vibration of track-embankment-ground system induced by high-speed trains moving on the track system was simulated using this method. Special attention was given to the dynamic responses including the time and frequency domains for the track-ballast-embankment-ground system.

2. Validation of finite element simulation in a homogeneous half-space

2.1 Creation of finite element simulation model

The elastically distributed wheel load was simulated by Krylov *et al*. (1994) and Krylov (1995). However, the effect of varying speeds at which the vehicles were traveling was not considered in those studies. The response of a viscoelastic half-space subjected to moving loads with static and dynamic components was investigated by Hung and Yang (2001). Four types of vehicle loads were considered, including moving point load, uniformly distributed wheel load, elastically distributed wheel load, and a train load simulated as a sequence of elastically distributed wheel loads. Hall (2003) created a dynamic 3D FEM with moving loads to simulate train-induced ground vibrations. The dynamic response of a railway track with a moving train was studied employing a three-dimensional model for the track by Vostroukhov and Metrikine (2003). The train load has been simulated through a set of vertical point loads applied on the beams. The structure was excited by eight-point loads of constant amplitude P that move along the beams at a constant speed. These loads stood for the weight of a train wagon disregarding dynamic variation of the contact force.

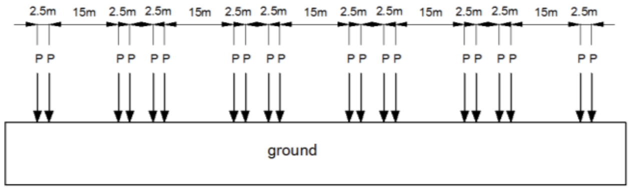

Fig. 1 Axle unit load mode

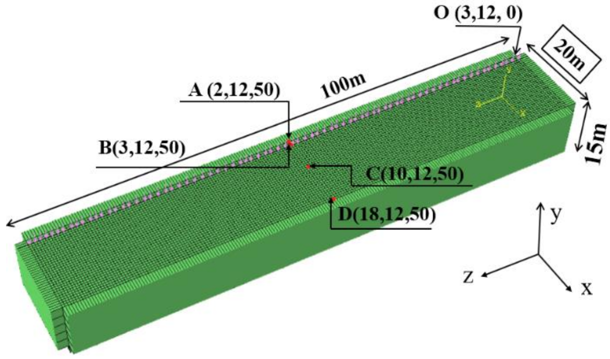

Fig. 2 Finite element meshes of the three-dimensional ground model

Table 1 Equivalent-linear material parameters

Elasticity modulus	Poisson's Ratio	Density	P wave	S wave	Rayleigh wave
E (MPa)	μ	ρ(kg/m^3)	V_P (m/s)	Vs (m/s)	V_R (m/s)
35	0.3	1800	161. 8	86.5	80.0

In this study, a finite element approach is presented to study the ground vibration characteristics. First, the moving train load was approximately represented using a series of equivalent distribution forces vertically acting on the loading elements in a half-space. The LK Infinite elements with reference to the work conducted by Lysmer and Kuhlemeyer (1969) and Kouroussis *et al*. (2009) and Kouroussis *et al*. (2011) were used to represent the infinite boundary condition of the soil ground. The explicit central difference method was adopted for time integration of the dynamic equilibrium equations.

In the loading model presented by Hall (2003), the rail was composed of nodes and beam elements. In the following, the nodes in the rail referred to loading nodes. Every fifth loading node was connected with the beam elements to form the sleepers. At the loading nodes, point loads were applied. In this study, a unit distribution load P moving at a speed of 60, 80, 100, 120 m/s in an elastic half-space is considered. The axle load acting on the unit element (ΔS) of the ground is (F = 70 KN). The area of the unit element is ΔS = 0.5 m*0.1 m = 0.05 m^2, and the unit distribution is P = F/ΔS = 1.4 MPa. An appropriate time and frequency domain analysis method was used to examine the vibration effects of the ground under the moving loads and demonstrate the capabilities of the proposed finite element model. The axle unit load modes of single, double, four, and twenty loads are shown in Fig. 1. The distance between every load is also shown.

For the sake of symmetry, only half of the finite element model is built in Fig. 2. The model was 100 m in length, 20 m in width, and 15 m in height and consisted of 43065 elements. The interior domain of the model was uniformly meshed using 8-node cubic hexahedral elements with reduced integration and hourglass control. The center, symmetry boundary, and outside boundary of the model were restrained in the horizontal direction. The fixed and infinite element boundaries were employed in numerical simulation. The nodes at the bottom boundary were fixed in every direction to simulate the bedrock. Table 1 shows the values of density, Poisson's ratio, ground Rayleigh wave speed V_R.

This section carries out a preliminary study on the influence of load travelling speed on the ground vibration characteristics. The load moving speeds selected were 60, 80, 100, and 120 m/s. Because the ground Rayleigh wave speed is assumed to be 80 m/s, the selected load moving speeds are in the subcritical, critical, and supercritical ranges. In this 3D FEM, the equivalent uniform loads were represented in the half-space. Four representative points A (2, 12, 50), B (3, 12, 50), C (10, 12, 50), and D (18, 12, 50) in the model were selected. The moving load point started at the position (3, 12, 0) and moved along the Z-direction at a constant speed. Fig. 1 shows the four load modes including single load, double load, four-load, and twenty-load. They were considered in the finite element simulation to examine the ground vibrations.

In this section, three different dynamic boundaries, namely, fixed boundary (FIX), infinite boundary (INF), and infinite with damping boundary (DINF), were adopted to examine the dynamic absorption efficiency of damping and infinite elements. Rayleigh damping was considered to represent energy-dissipating mechanisms in the simulation. The mass α and stiffness proportional damping β were in the values of 1.4 and 0.00024, respectively. They provided slight damping ratios of 2-4% in the frequency range of 3-50 Hz.

2.2 Validation of the finite element simulation

2.2.1 Verification and selection of dynamic boundaries

Fig. 3 shows the time and frequency analysis of the dynamic velocity at point A under a single axle load travelling at a speed of 80 m/s in 3D FEM with different boundaries. Fig. 3(b) shows the frequency spectrum amplitude of the velocity, which was computed using fast Fourier transform. In Fig. 3(a), the peak dynamic velocity for fixed boundary (FIX) was observed to be larger than that of the other boundaries of (INF) and (DINF). The fluctuations of dynamic velocity decreased for all three with time. The maximum velocities for FIX, INF, and DINF were 0.09, 0.056, and 0.044 m/s, respectively. For boundaries of INF and DINF, the maximum velocity amplitude decreased by 37.7% and 51%, respectively. The dynamic absorption efficiency of the damping and infinite elements can also be found in Fig. 3(b). For different boundaries, the frequency spectrum amplitude of dynamic velocity tended to decrease. The maximum velocity spectrum amplitudes for FIX, INF, and DINF were 0.009, 0.0039, and 0.0035 m/s/Hz, respectively. For the boundaries

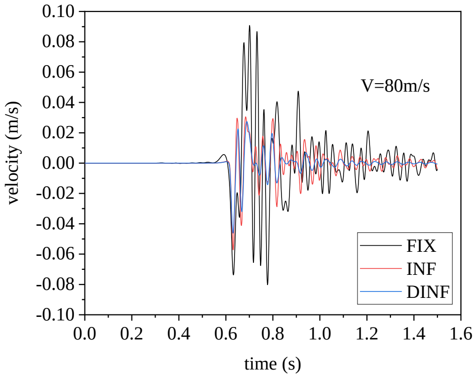

(a) Velocity amplitude

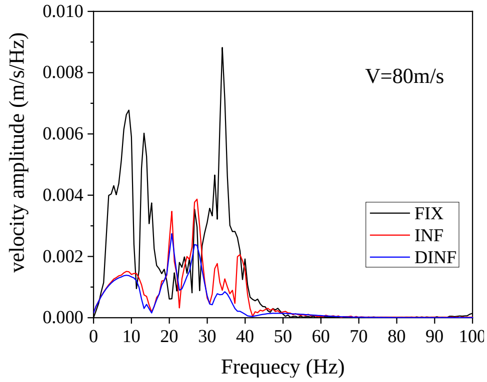

(b) Velocity spectrum amplitude

Fig. 3 Time and frequency analysis of velocity at point A under the single unit load moving at a speed of 80 m/s

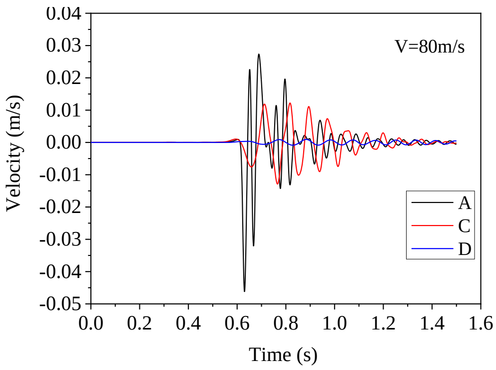

(a) Velocity amplitude

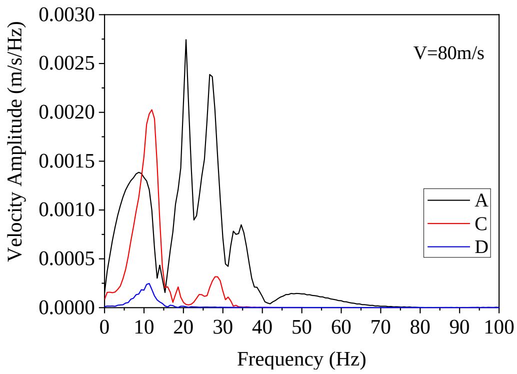

(b) Velocity spectrum amplitude

Fig. 4 Time and frequency analysis of velocity at points A, C, and D under single unit load moving at a speed of 80 m/

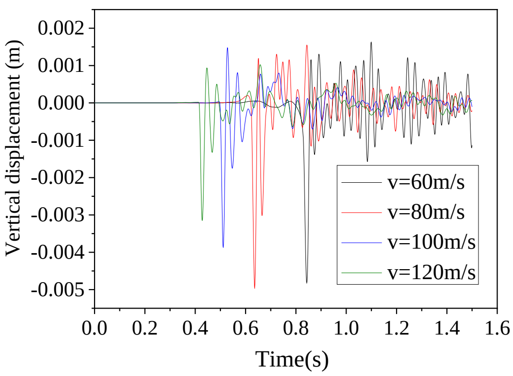

(a) Single load mode

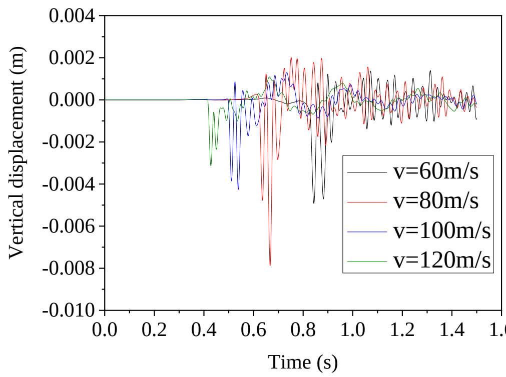

(b) Double load mode

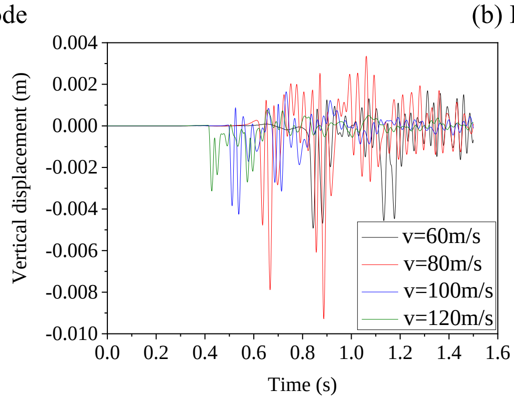

(c) Four-load mode

Fig. 5 Time histories of vertical displacement at point B for three train load modes

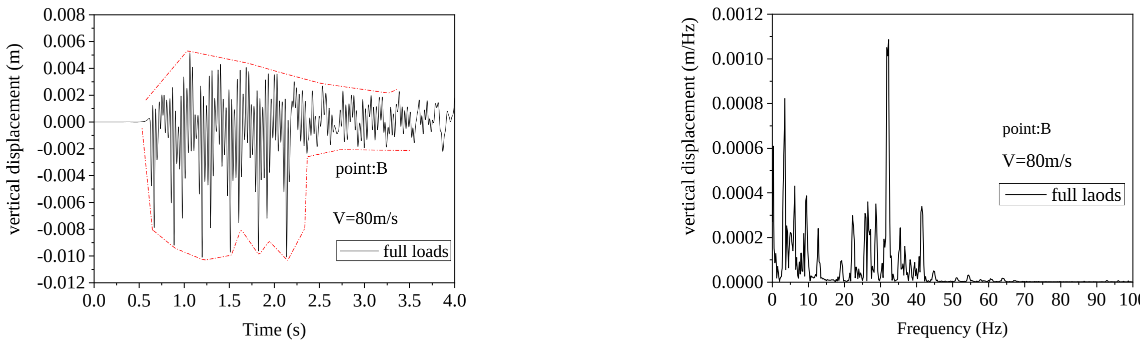

(a) Velocity amplitude (b) Velocity spectrum amplitude

Fig. 6 Time histories and frequency spectrum curves of the vertical displacements at point B of the twenty-load mode moving at a speed of 80 m/s

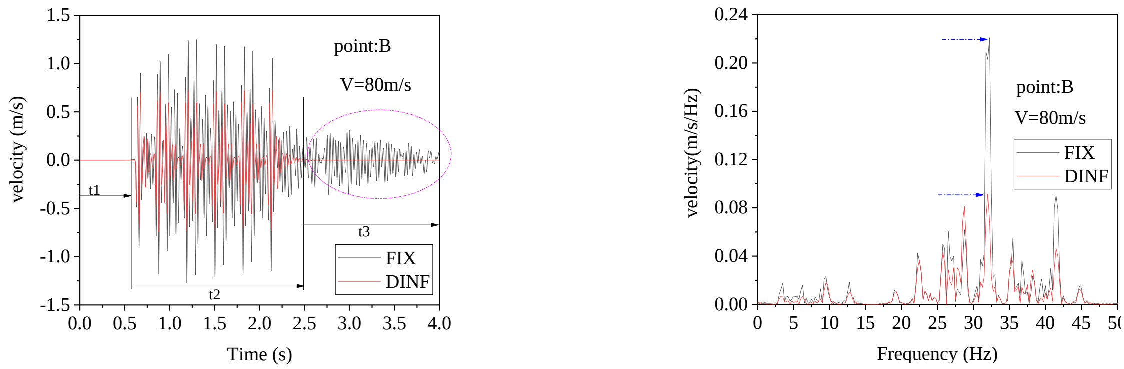

(a) Velocity amplitude (b) Velocity spectrum amplitude

Fig. 7 Time histories and frequency spectrum curves of velocity at point B for the twenty-load mode (full train load mode) moving at a speed of 80 m/s

of INF and DINF, the vibration response amplitudes were reduced by 57% and 61%, respectively. Accordingly, it is evident that the LK infinite elements used to represent the infinite boundary condition can effectively absorb S and P waves. Material damping can also reduce the amplitude of the vibration response.

Four representative points of A (2,12,50), B (3,12,50), C (10,12,50), and D (18,12,50) in the established model were selected in Fig. 2. The unit moving load point started at the position (3, 12, 0) and moved along the line marked with purple towards the Z-direction at a constant speed, crossing the point B. Fig. 4 displays the time and frequency analysis of dynamic velocities at points A, C, and D under the single unit load travelling through ground surface with a DINF boundary at a speed of 80 m/s. In Fig. 4(a), the dynamic velocity amplitude decreased with the increase of the distance away from point of B. The intervals between points A, C, D and point B are 1, 7, and 15 m, respectively. The dynamic frequency spectrum amplitude also decreased with the rise of the distance away from point B. The location of peak frequency amplitude tended to move from the medium frequency area (10 to 30 Hz) to the low frequency area (0 to 10 Hz).

2.2.2 Dynamic response superposition effect of moving loads

Fig. 5 (a) expresses the time history of vertical displacements at point B (3,12,50) under the single the unit load travelling at four various speeds. It was observed that the downward peak displacement roughly coincides with the instantaneous position of the moving loading point at different train speeds. The vertical displacement increased with moving load speed and tended to fall after reaching a maximum value. It is clearly shown in Fig. 5(b) that the peak displacement at point B is around 0.005 m at a train speed of 60 m/s for the double load mode. The peak displacement at point B reached 0.008 m when the train speed was equal to the ground Rayleigh wave speed of 80 m/s, and tended to drop with a rise in train load speed. For the double load mode, the peak displacement was around 0.003 mm at a train speed of 120 m/s and it was reduced by about 62.5% compared to the corresponding value determined at a train speed of 80 m/s. In particular, the peak displacement increased by 40% at the train speed of 80 m/s as the load mode varied from single load to double load. In Fig. 5(c), the peak displacement for the four-load mode at the same speed increased by around 47% in comparison with that of the single load mode.

For the double and four-load modes, the downward peak displacement roughly coincided with the instantaneous position of the moving loading point at different train speeds. This coincidence gradually moved out of phase as the train speed increased. The maximum ground displacement increased with the load moving speed, attained a maximum value at the critical speed of 80 m/s, but then decreased afterwards. The maximum value is believed to coincide with the velocity of the fundamental mode for the surface wave in the ground system. Owing to the superposition and compounding of the adjacent loads, the first set of loads affects the dynamic response induced by the second set of loads. This difference originates from the vibration superposition interference among moving loads. The dynamic response and vibration superposition interference have been greatly changed and reconstructed repeatedly.

2.2.3 Full train loads mode

Fig. 6 exhibits the time history and frequency curves of the vertical displacement at point B with the twenty-load mode moving at a train speed of 80 m/s. In Fig. 6(a), this mode together with single, double and four-load modes lead to a similar ground vibration response. The first set of loads influenced the subsequent dynamic response induced by the second set of loads. These vibration waves induced by moving loads resulted in either a decrease or an increase in the maximum vertical displacement of ground in the cases of single, double and four-load modes. As it is shown in Fig. 6(b), the peak vertical displacement at point B occurred between 0 and 45 Hz for the twenty-load or the full train load mode. This tendency corresponded well to the ground vibration characteristics.

Fig. 7 displays the time histories and frequency spectrum curves of velocity at point B for the twenty-load mode moving at a speed of 80m/s. Two boundary conditions were simulated to investigate the efficiencies of the damping and infinite element boundary. As it is shown in Fig. 7(a), the peak velocity with DINF boundary was lower than that with FIX boundary. The vibration responses were different at periods of t1, t2, and t3. The vertical velocity occurred after t1, fluctuating with the loads moving along the Z-direction. It was observed that the vertical velocity decided with DINF boundary decreased into a very low level at period t3, and was much lower than that with FIX boundary. The ground vibration attenuation effect was well captured using this dynamic simulation method. Similar varying tendencies of frequency amplitude attenuation are also seen in Fig. 7(b). The peak velocity amplitude with DINF boundary was lower than that with FIX boundary. A possible explanation is that the DINF boundary can absorb more vibration energies, such as P and S waves, in ground soil.

In this section, numerical results for the vibrations of the ground surface are presented for various modes of train loads moving on ground with different speeds over and below the Rayleigh wave speed of ground soil. Because the ground vibration is very large when the speed of moving load is identical to the Rayleigh wave speed of ground, it is significantly important to reduce the soil vibration induced by high-speed trains. The results verified that the established analytical model is suitable to investigate the dynamic response of ground at all important frequencies.

3. 3D FEM modelling and analysis of track-embankment-ground system

3.1 3D FEM model of track-embankment-ground system

Fig. 8 shows the axle load and geometry of a five-

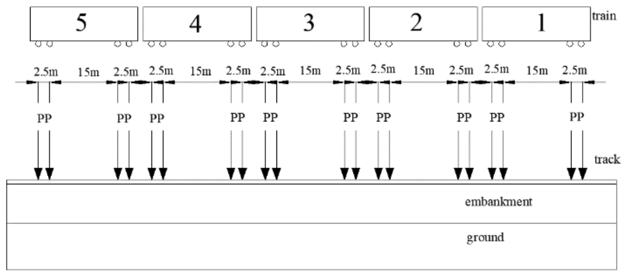

Fig. 8 Geometry and axle loads of the five-carriage train

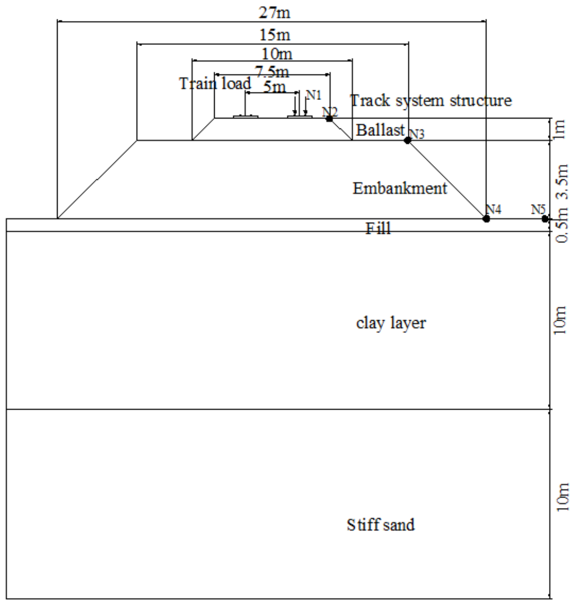

Fig. 9 Geometry of track-ballast-embankment and ground

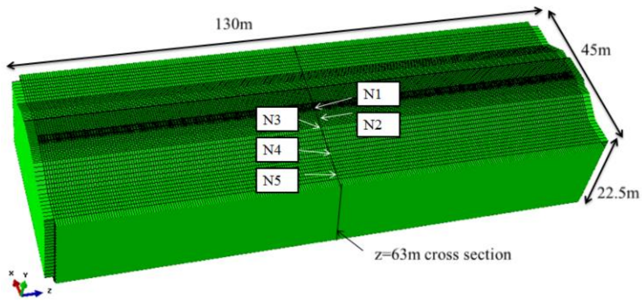

(a) 3D view

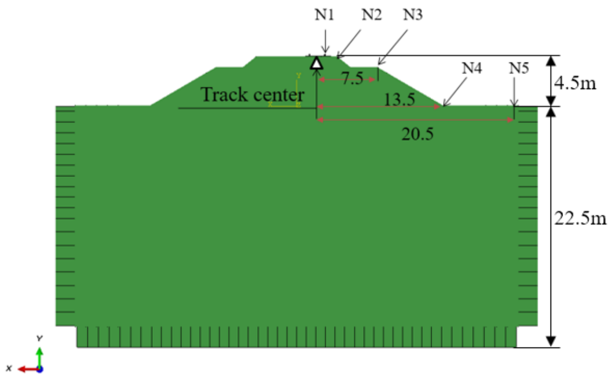

(b) Cross section

Fig. 10 Finite-element mesh of the track-ballast-embankment and ground

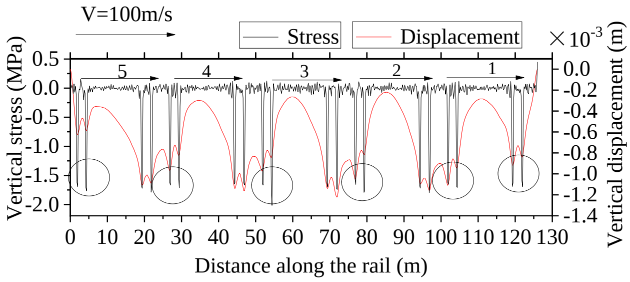

Fig. 11 Dynamic response of rail in typical time at a train speed 100 m/s at 1.22 s

Table 2 Material parameters of the finite simulation

Material	*E(MPa)*	μ	$\rho(kg/m^3)$	V_S	V_R
Ballast	389	0.3	2200	260.8	241.9
Embankment	250	0.3	1800	231.1	214.4
Fill	90.75	0.3	1800	138.7	128.6
Clay	25.36	0.35	1600	76.6	71.6
Stiff sand	100	0.3	1800	146.2	135.6
Rail	210000	0.17	7800	3392	3074.2
Sleeper	20000	0.2	2500	1826	1664.5

Note: E is Young's modulus; ρ is density; μ is Poisson's ratio; V_S and V_R are shear and Rayleigh wave speeds, respectively

carriage train. The moving train loads were applied on the rail. The rail was divided into small units (element). The loading area ΔS was 0.02 m^2. For CRH380A produced in China, F is 70 kN, representing an axle load of 14 t. The load distribution P was subjected to a wheel load F = 70 kN and moved on the elements at a specific speed along the rail. The load distribution P was calculated as the ratio of the train axle load F and element ΔS. It is expressed using Eq. (1)

$$P = \frac{F}{\Delta S} \tag{1}$$

Thus, the calculated distribution load P was 3.75 MPa. The load P was then applied directly on the rail elements with the time shifts corresponding to the train speed.

Fig. 9 shows the geometry of track-ballast-embankment-ground system. The heights of the embankment and the ballast were 3.5 and 1 m, respectively. The depths of both the clay and the stiff sand layers were 10 m (Sun *et al.* (2006), Wu *et al.* (2013), Wu *et al.* (2018), Yoshimoto *et al.* (2016), Winter *et al.* (2017), Wu *et al.* (2019), Ma *et al.* (2019)). Some representative positions, such as rail top (N1), ballast (N2), embankment top (N3), embankment foot (N4), and ground surface (N5), were selected to investigate the dynamic response of the track-embankment-ground system. The distances between those selected points and the track center line were 1.2, 3.75, 7.5, 13.5, and 20.5 m.

In Fig. 10, the model was set to be 130 m in length. The 3D model, consisting of rails, sleepers, ballast, and embankment, was 45 m × 130 m × 27 m and contained 306,668 elements. The fixed boundaries were used at the bottom of the model. Infinite elements (CIN3D8) based on the previous work by Lysmer *et al.* (1969) were used as the boundaries in the X and Z directions to represent the infinite boundary condition to absorb S and P waves. The nodes at the bottom boundary were fixed in every direction to simulate the bedrock. Both ends of the ground boundary at the Z-direction were fixed in every direction in order to keep the ground stationary and in place. The parameters for finite element simulation are found in Table 2.

3.2 Analysis of vibration response characteristics of track-ballast-embankment-ground system

The dynamic responses of the track-embankment-ground system were computed and analyzed. Fig. 11 shows the instantaneous dynamic response of the rail for a train moving at a speed of 100 m/s for 1.22 s. It was observed that the peak vertical displacement and the stress along the rail top roughly coincided with the instantaneous position of the moving loading point. The distribution of the peak vertical displacement corresponding to the dynamic stress was different from that of the quasi-static state. The vertical displacements of the rail induced by the train load at quasi-static state were the same. The peak vertical displacement under each train load was the same from each other. However, for the dynamic condition, the peak vertical stress appeared at about 1.6 to 1.75 MPa. The peak vertical displacements induced by the different carriages were different from each other. This is attributed to the superposition effect of the vibration induced by the train moving loads on the rail.

Fig. 12 shows the vertical displacement contours of the embankment at different times at a train speed of 100 m/s. The instantaneous vibration displacement U2 (elastic vibration) was generated once the initial moving load on the vehicle entered the track area. Subsequently, the vibration load transferred into the surrounding area, forming the distribution of vibration displacements in Fig. 12(a). The

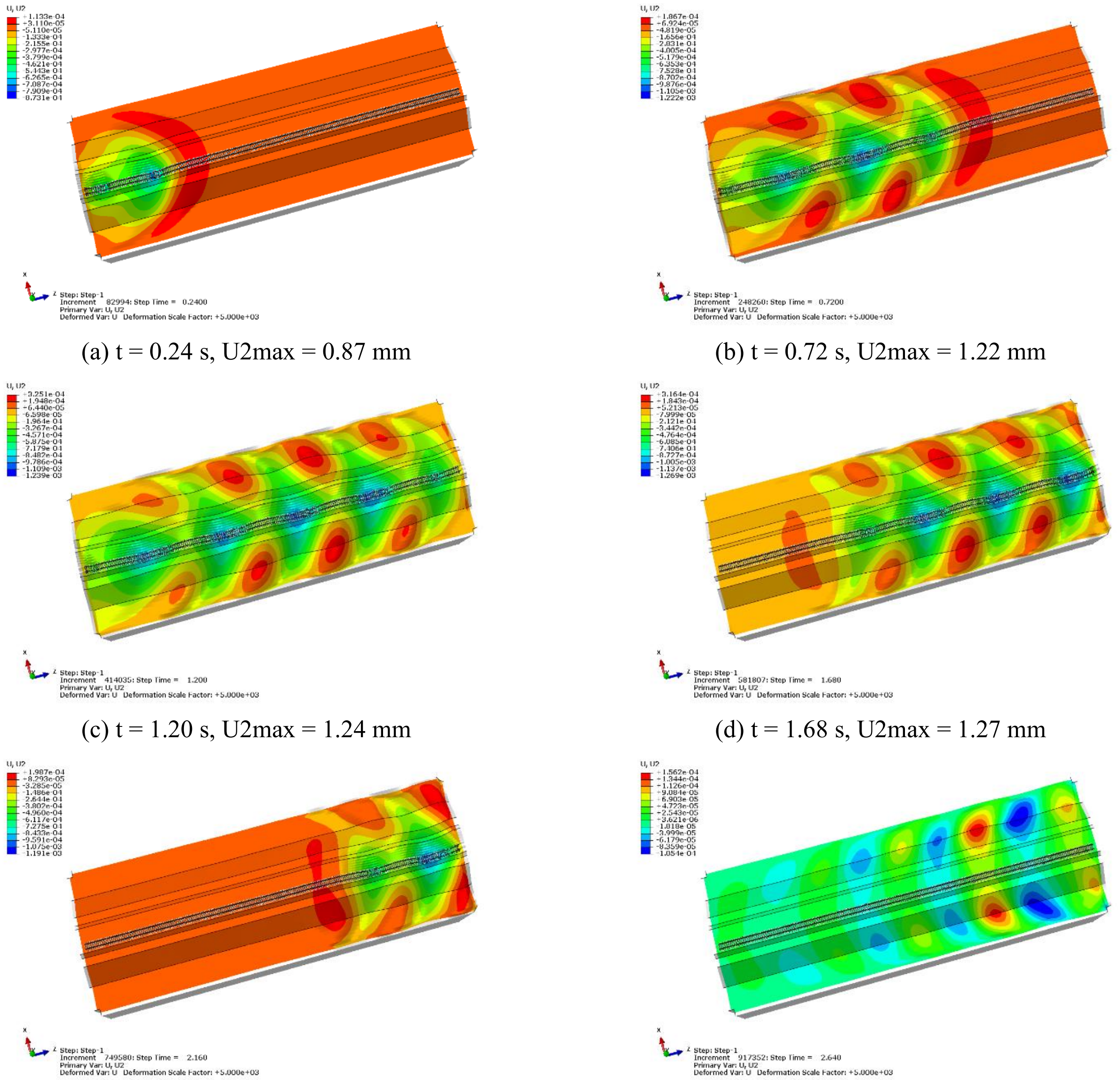

(a) t = 0.24 s, U2max = 0.87 mm
(b) t = 0.72 s, U2max = 1.22 mm
(c) t = 1.20 s, U2max = 1.24 mm
(d) t = 1.68 s, U2max = 1.27 mm
(e) t = 2.16 s, U2max = 1.19 mm
(f) t = 2.64 s, U2max = 1.05 mm

Fig. 12 Contours of the vertical displacement of embankment magnified by a factor of 5000 at different times for a train speed of 100 m/s travelling from left to right

vibration displacement varied dynamically with the movement of the loads. In Fig. 12(b), more train wheel loads entered the track area with time, generating continuous displacement response in the track, foundation bed, and foundation. The vibration displacement gradually decreased from the track center (vibration resource) outwards. The maximum vertical displacement (U2max) increased as train loads passed by. In Fig. 12(d), the U2max was close to 1.27 mm at the time 1.68 s. The vibration amplitude and range decreased gradually as the moving loads passed from t = 2.16 s to t = 2.64 s, as shown in Figs. 12(d)-12(f). The maximum vertical displacement U2max reduced by 0.22 mm.

Figs. 13(a)-13(d) show the vertical displacement contours of embankment magnified by a factor of 5000 at different train speeds of 60, 80, 100, and 120 m/s travelling from left to right. The maximum vertical displacements attained 1.15, 1.17, 1.24, and 1.34 mm at four increasing levels of speed. The displacements increased simultaneously and rapidly with train speeds.

The vibration displacement curve was similar to vibration waveform. Once the train load speed exceeded the vibration propagation velocity of the ground, the wave induced by the train loads spread out as the train moved. It was seen that the wave propagation is not perpendicular to the moving loads. As a form of expression of vibration wave fronts, the equipotential line shapes of displacement distribution, gradually varied with different load speeds. The equipotential line shapes varied from round to oval, similar to the shape of water wave generated from a water speedboat. Similar results were reported from a 3D train model subjected to moving point loads in the previous work conducted by Hall (2003), Galvín (2007) and El Kacimi *et al*. (2013).

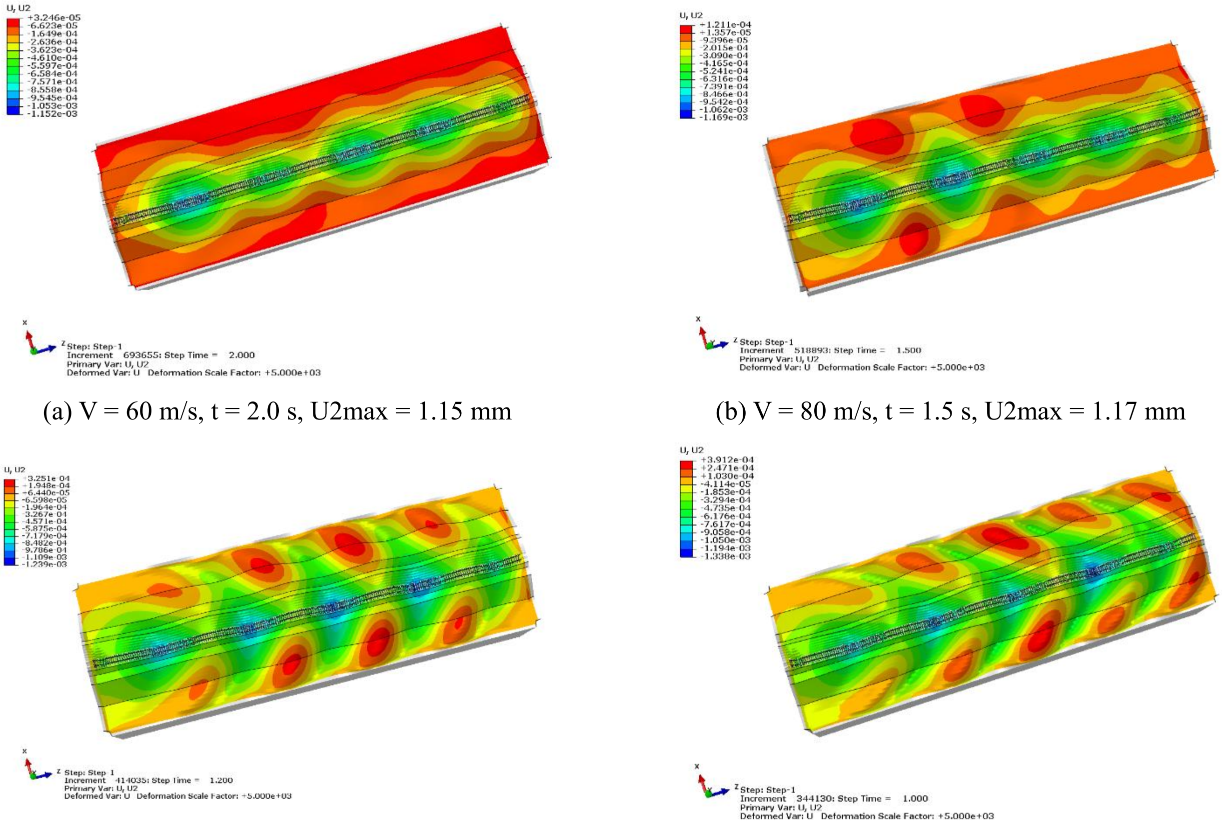

(a) V = 60 m/s, t = 2.0 s, U2max = 1.15 mm

(b) V = 80 m/s, t = 1.5 s, U2max = 1.17 mm

(c) V = 100 m/s, t = 2.16 s, U2max = 1.24 mm

(d) V = 120 m/s, t = 1.0 s, U2max = 1.34 mm

Fig. 13 Contours of the vertical displacement of embankment magnified by a factor of 5000 at different train speeds for a train travelling from left to right

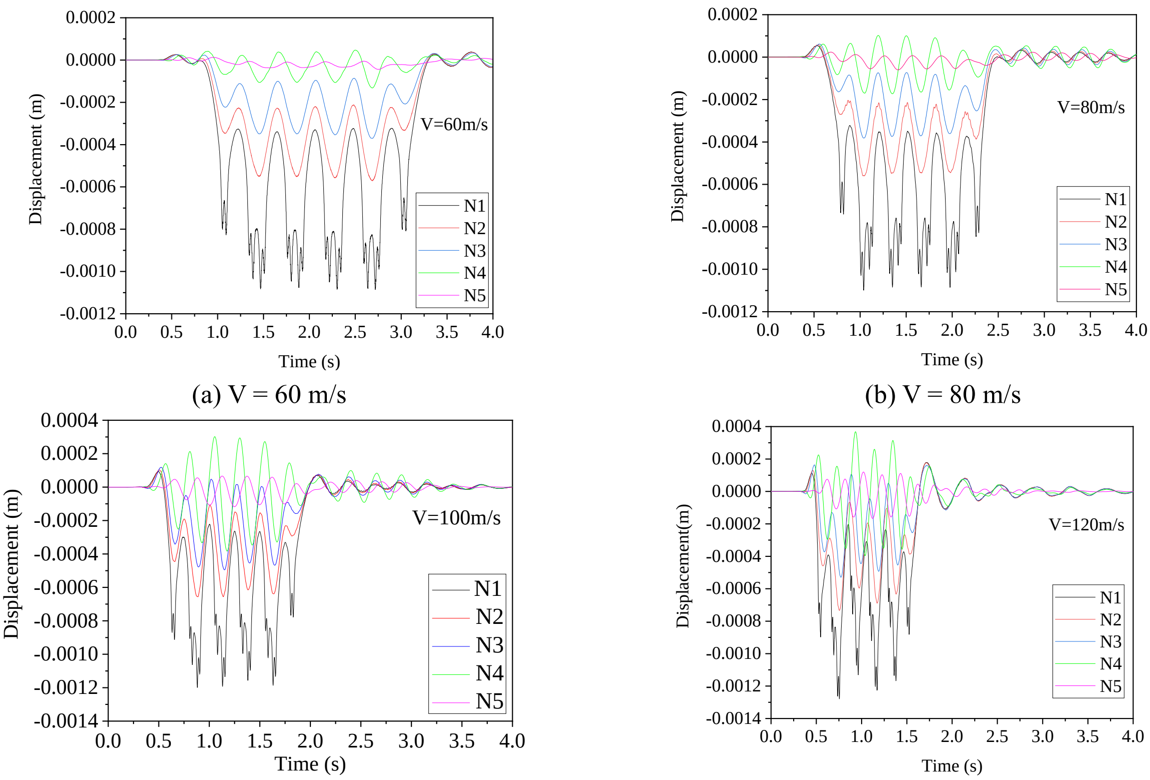

(a) V = 60 m/s

(b) V = 80 m/s

(c) V = 100 m/s

(d) V = 120 m/s

Fig. 14 Time histories curves of vertical displacement for points N1 to N5 at four different train moving speeds

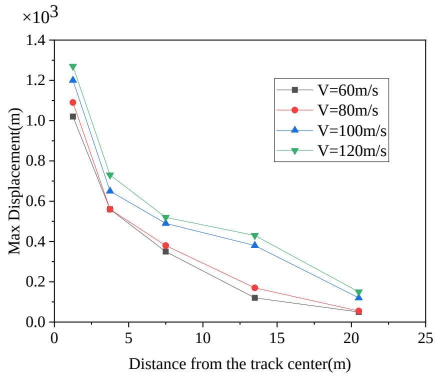

Fig. 15 Comparison of maximum vertical displacements for points N1 to N5 at four different train moving speeds

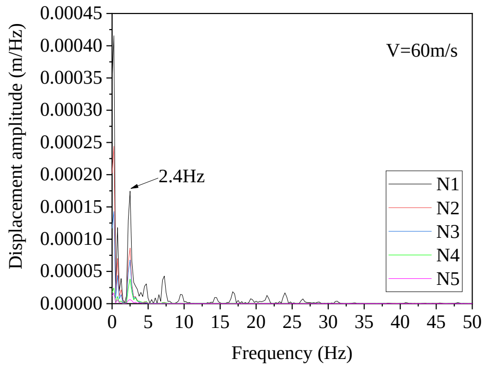

(a) V = 60 m/s

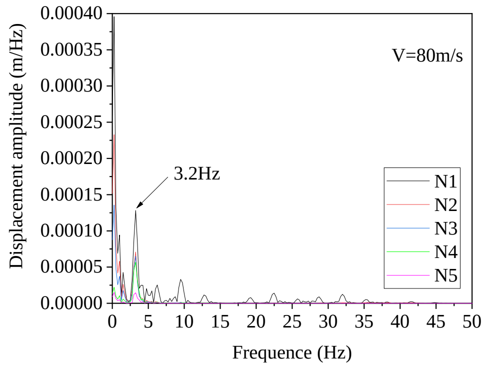

(b) V = 80 m/s

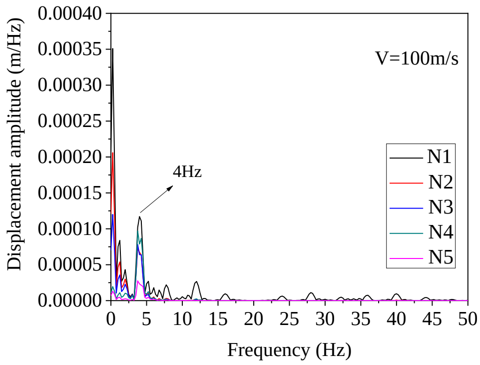

(c) V = 100 m/s

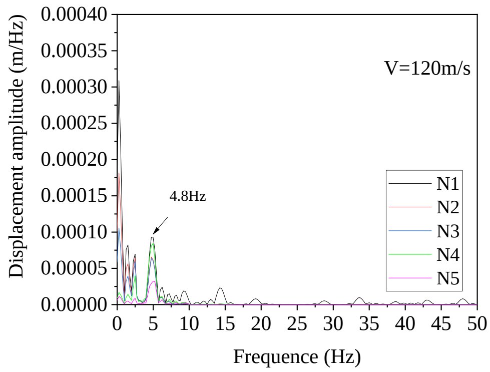

(d) V = 120 m/s

Fig. 16 Frequency amplitude spectrum curves of vertical displacement for points N1 to N5 at different train moving speeds

It was seen that the appetence and attenuation of the vibration displacement response were fast as the train progressed. The vibration displacement generated by the train moving load in the structure under track is mainly transient elastic displacement. Meanwhile, the dynamic stiffness characteristics of the offline structure governed the level of vibration response.

3.3 Dynamic response analysis in time and frequency domain

Fig. 14 shows the vertical displacement time histories at five representative locations denoted by N1 to N5 in Figs. 9 to 10. They were 1.2, 3.75, 7.5, 13.5, 20.5 m away from the track center. As shown in Figs. 14(a) to (d), the vibration displacement curve of N1 on the track corresponds to the geometric position of the load at different train moving speeds. With a rise in the distance from the track center, the vibration displacement curves of N2 to N5 gradually exhibited the form of sine wave. The vibration displacements induced by train loads were apparent for N1 near the track center. The vertical displacement at N1 was larger than that those at other points. The peak displacement at the selected point decreased with the distance from the track center (vibration source). The vibration wave field generated by the train load was controlled by the vibration characteristics of track-ballast-embankment-ground system. For node N4, the surface waves induced by train loads moved to the embankment toe, and was influenced by the changes in geometry and medium. A vibrational resonance phenomenon occurred at point N4 in the form of a vertical displacement. The vibration waves induced by train loads were greatly influenced by a weakening effect of the sloping surfaces on the ballast and embankment.

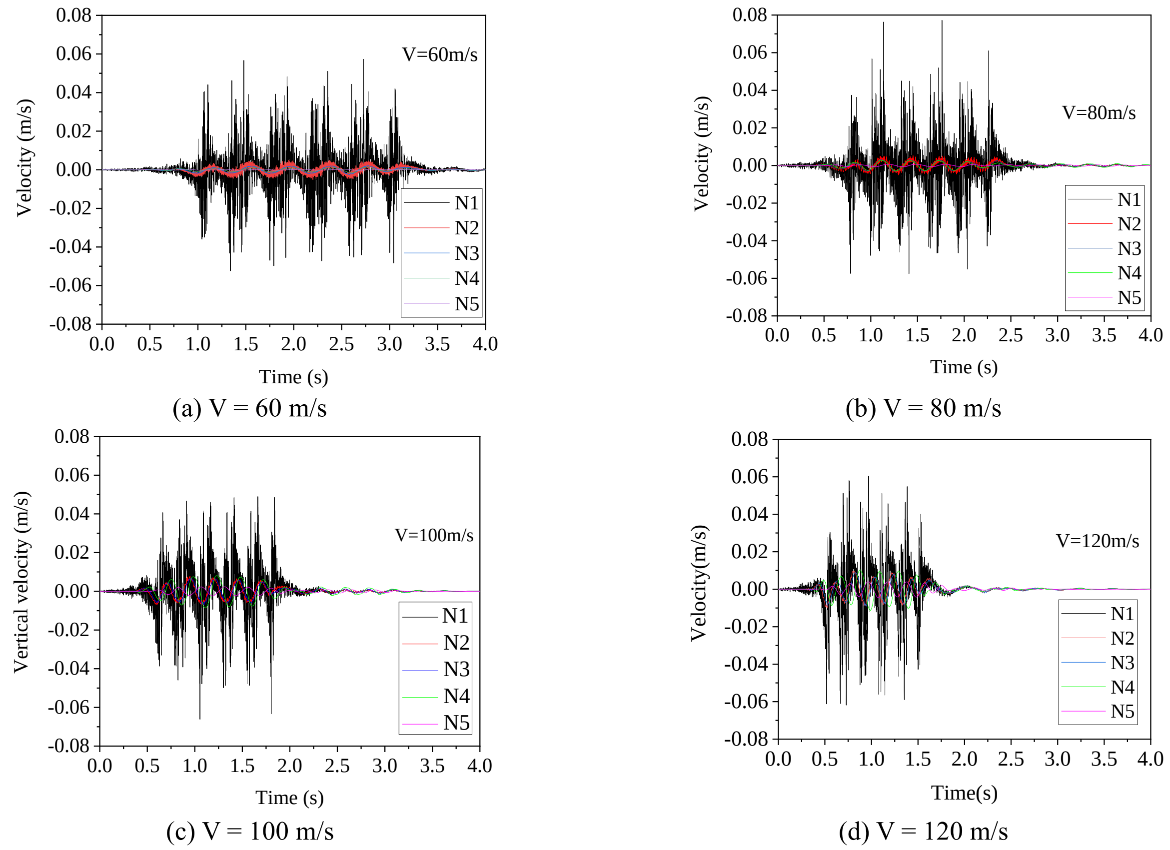

Fig. 17 Time history curves of vertical velocity for points N1 to N5 at four different train moving speeds

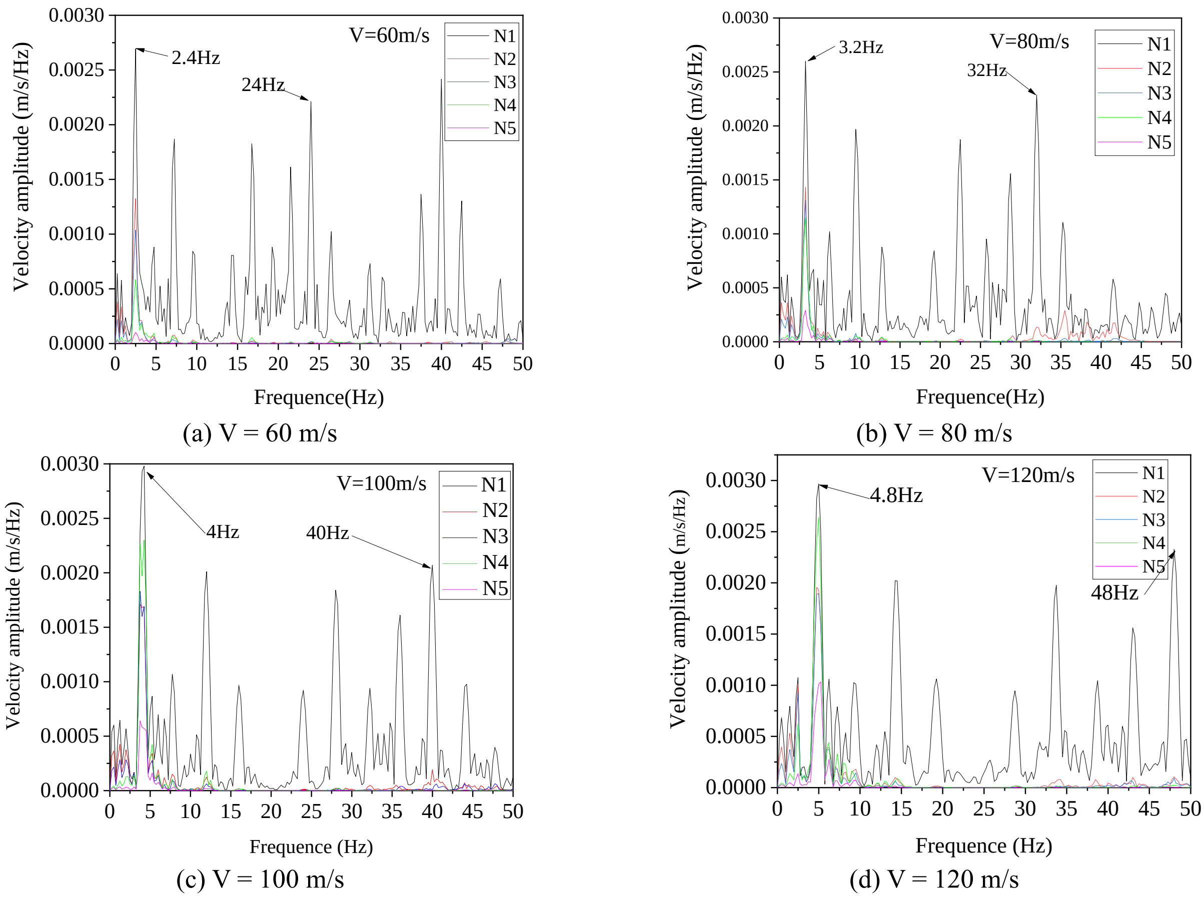

Fig. 18 Frequency amplitude spectrum curves of vertical velocity for points N1 to N5 at different train moving speeds

Fig. 15 displays the maximum vertical displacements for points N1 to N5 at four different train moving speeds. For all points, the maximum vertical displacements increased with the train speed and decreased with the increasing distance from the track center (vibration source) at four train speeds. The impact of velocity variation on the vibration displacement was minimal. The maximum vertical displacement for N1 was larger than that for N2, N3, N4, and N5. For V = 80 m/s, the maximum vertical displacements for N1 to N5 were 1.09, 0.56, 0.38, 0.17, and 0.055 mm, respectively. For N2, N3, N4, and N5, the attenuation rates were 48.6%, 65.1%, 84.4%, and 95%. The attenuation tendency became much faster as the distance from vibration center increased. The vibration energy was largely reduced near the track center.

Fig. 16 shows the amplitude spectra curves of the vertical displacement at points N1 to N5 at four different train moving speeds. These values were computed and obtained using fast Fourier transform. The frequency spectrum curve of vertical displacement for each point was apparent. The frequency range lower than 0.3 Hz represents the quasi-static response component induced by train loads. A frequency range larger than 0.3 Hz refers to the dynamic response component induced by inertial effects associated with the train speed, axle distance, bogie distance and carriage length. In this study, the carriage length was 25 m, the train speed was 100 m/s (360 km/h), and the passage frequency of the carriage was 4 Hz. Fig. 16(c) displays that the maximum velocity amplitudes appeared for all observation locations at the frequency of 4 Hz. The spectrum amplitude for N1 was larger than that for N2 to N5. With the increase in the distance from the vibration source, the spectrum amplitude for the observed point decreased accordingly. As seen in Figs. 16(a), (b), and (d), the passage frequency of displacement amplitude spectra were 2.4, 3.2, and 4.8 Hz at train speeds of 60, 80, and 120 m/s. The displacement amplitude increased linearly with the rise in train speed.

Fig. 17 shows the vertical velocity time histories at the train speeds of 60, 80,100, and 120 m/s. For different train speeds, vibration speeds exhibited similar vibration response tendency. The superposition and attenuation of vibration velocities appeared in company with the passing of train loads. It vanished gradually with the leaving of moving loads. The response of vibration velocity was instantaneous, and the delay of attenuation was minimal as the train load passed and then became rapid as the train load moved away. For V = 100 m/s, vertical velocity at point N1 represented the vibration responses near the track and the sleeper. The positive and negative values of the peak velocities were 0.049 m/s and -0.065 m/s, respectively. The dynamic attenuations of velocity were rapid when the vibration waves entered into the track-embankment-ground system. The peak velocities at points N2 to N5 were lower than that of point N1, and the maximum value among them was only about 0.008 m/s.

Fig. 18 expresses the frequency amplitude spectra of vertical velocity for points N1 to N5, which were obtained using fast Fourier transform. The frequency spectra curves for points N2 to N5 contained significant frequencies less than 5 Hz, while the frequency spectra for N1 covered a wider range of significant frequencies. For V = 100 m/s, the frequency spectra for point N1 showed the peak values in bogie passing frequency (4 Hz) and axle load passing frequency (40 Hz). It showed peak values at low and intermediate frequencies, corresponding to the dominant bogie and axle passage peaks. These resulted from the composite dynamic characteristics of track structure. Similar tendency was obtained for velocities equal to 60 and 120 m/s as shown in Figs. 18(a) and (d). With the exception of point N1, the vibration velocity response energy was mainly distributed in the middle and low frequency regions, which were composed of ballast, embankment, and soil ground. The numerical model was capable of properly simulating the vibration response and its distribution of the substructure under train moving loads.

4. Conclusions

A finite element model was developed to analyze the vibration characteristics of the embankment and ground induced by high-speed train loads. The finite element simulation was initially validated and extended to three-dimensional space to examine the ground vibrations induced by high-speed train loads passing through the ground surface. By means of the 3D finite element simulation, the dynamic response of track-embankment-ground system was simulated and analyzed. The proposed numerical model has the ability to reproduce the dynamic response of track-ballast-embankment-ground system at all important frequencies. The LK infinite elements representing the infinite boundary condition can effectively absorb S and P waves. Material damping can also reduce the amplitude of vibration response. It was confirmed that both LK infinite elements and material damping are suitable in complex 3D dynamic simulation calculation.

The surface wave fields generated by moving trains at high speeds were clearly reproduced. The peak displacement and stress along the rail top roughly coincided with the instantaneous position of the moving loading point. The distribution of the peak displacement corresponding to dynamic stress under the train moving loads was different from that of a quasi-static state. There were vibration attenuations in the wave fronts as the stresses transited from ballast to embankment, and from embankment to ground. This phenomenon is a consequence of the damping effects of the ballast, embankment, and ground. The vibration waves induced by train loads were greatly influenced by a weakening effect of the sloping surfaces on the ballast and embankment. Theses tendencies were significant when the vibration waves are at medium and high frequencies. Thus, the vibration amplitude outside the embankment was significantly reduced.

The attenuation of vibrations along the cross-section of the track was slightly affected by the train speed. The maximum vertical displacements decreased as the distance from the track center (vibration source) increased. The variation in velocity minimally impacted the vibration response.

A frequency amplitude spectrum analysis of the vibration response induced by high-speed train loads indicated that the peak frequencies of the vibration response of the track structure were related to the geometric parameters of trains. The main peak frequencies were located in the area of low and intermediate frequencies, corresponding to the dominant bogie and axle passage peaks. These are results of the composite dynamic characteristics of track structure.

Acknowledgments

A part of the work was supported by National Key Research and Development Program of China (2016YFC0800205), National Natural Science Foundation of China (51908152, 51908153, Key Project 51438004), Guangzhou city Technology and Science Program (201904010278).

References

Auersch, L. (2008), "The effect of critically moving loads on the vibrations of soft soils and isolated railway tracks", *J. Sound Vib.*, **310**(3), 587-607. https://doi.org/10.1016/j.jsv.2007.10.013.

Bian, X., Cheng, C., Jiang, J., Chen, R. and Chen, Y. (2016), "Numerical analysis of soil vibrations due to trains moving at critical speed", *Acta Geotech.*, **11**(2), 281-294. https://doi.org/10.1007/s11440-014-0323-2.

Bian, X., Jiang, H., Chang, C., Hu, J. and Chen, Y. (2015), "Track and ground vibrations generated by high-speed train running on ballastless railway with excitation of vertical track irregularities", *Soil Dyn. Earthq. Eng.*, **76**, 29-43. https://doi.org/10.1016/j.soildyn.2015.02.009.

Cai, Y., Sun, H., and Xu, C. (2008), "Response of railway track system on poroelastic half-space soil medium subjected to a moving train load", *Int. J. Solids Struct.*, **45**(18-19), 5015-5034. https://doi.org/10.1016/j.ijsolstr.2008.05.002.

Cai, Z. and Raymond, G.P. (1994), "Modelling the dynamic response of railway track to wheel/rail impact loading", *Struct. Eng. Mech.*, **2**(1), 95-112. http://dx.doi.org/10.12989/sem.1994.2.1.095.

Chen, F., Wang, L. and Zhang, W. (2019a), "Reliability assessment on stability of tunneling perpendicularly beneath an existing tunnel considering spatial variabilities of rock mass properties", *Tunn. Undergr. Sp. Technol.*, **88**, 276-289. https://doi.org/10.1016/j.tust.2019.03.013.

Chen, Z., Yang, P., Liu, H., Zhang, W. and Wu, C. (2019b), "Characteristics analysis of granular landslide using shaking table model test", *Soil Dyn. Earthq. Eng.*, **126**, 105761. https://doi.org/10.1016/j.soildyn.2019.105761.

Cheshmehkani, S. and Eskandari-Ghadi, M. (2016), "Dynamic response of axisymmetric transversely isotropic viscoelastic continuously nonhomogeneous half-space", *Soil Dyn. Earthq. Eng.*, **83**,110-123. https://doi.org/10.1016/j.soildyn.2016.01.011.

Chong, S.H., Cho, G.C., Hong, E.S. and Lee, S.W. (2017), "Numerical study of anomaly detection under rail track using a time-variant moving train load", *Geomech. Eng.*, **13**(1), 161-171. http://doi.org/10.12989/gae.2017.13.1.161.

Correia, dos Santos, N., Barbosa, J., Calçada, R. and Delgado, R. (2017), "Track-ground vibrations induced by railway traffic: experimental validation of a 3D numerical model", *Soil Dyn. Earthq. Eng.*, **97**, 324-344. https://doi.org/10.1016/j.soildyn.2017.03.004.

Cui, C.Y., Zhang, S.P., Chapman, D. and Meng, K. (2018), "Dynamic impedance of a floating pile embedded in poro-visco-elastic soils subjected to vertical harmonic loads", *Geomech. Eng.*, **15**(2), 793-803. https://doi.org/10.12989/gae.2018.15.2.793.

El Kacimi, A., Woodward, P. K., Laghrouche, O. and Medero, G. (2013), "Time domain 3D finite element modelling of train-induced vibration at high speed", *Comput. Struct.*, **118**, 66-73. https://doi.org/10.1016/j.compstruc.2012.07.011.

Galvín, P. and Domínguez, J. (2007a), "Analysis of ground motion due to moving surface loads induced by high-speed trains", *Eng. Anal. Bound. Elem.*, **31**(11), 931-941. https://doi.org/10.1016/j.enganabound.2007.03.003.

Galvín, P. and Domínguez, J. (2007b), "High speed train-induced ground motion and interaction with structures", *J. Sound Vib.*, **307**(3-5), 755-777. https://doi.org/10.1016/j.jsv.2007.07.017.

Galvín, P., Romero, A. and Domínguez, J. (2010), "Fully three-dimensional analysis of high-speed train-track-soil-structure dynamic interaction", *J. Sound Vib.*, **329**(24), 5147-5163. https://doi.org/10.1016/j.jsv.2010.06.016.

Goh, A.T.C., Zhang, R., Wang, W., Wang, L., Liu, H. and Zhang, W. (2019), "Numerical study of the effects of groundwater drawdown on ground settlement for excavation in residual soils", *Acta Geotech.*, 1-14. https://doi.org/10.1007/s11440-019-00843-5.

Hall, L. (2003), "Simulations and analyses of train-induced ground vibrations in finite element models", *Soil Dyn. Earthq. Eng.*, **23**(5), 403-413. https://doi.org/10.1016/S0267-7261(02)00209-9.

Hino, J., Yoshimura, T., Konishi, K. and Ananthanarayana, N. (1984), "A finite element method prediction of the vibration of a bridge subjected to a moving vehicle load", *J. Sound Vib.*, **96**(1), 45-53. https://doi.org/10.1016/0022-460X(84)90593-5.

Hung, H.H. and Yang, Y.B. (2001), "Elastic waves in visco-elastic half-space generated by various vehicle loads", *Soil Dyn. Earthq. Eng.*, **21**(1), 1-17. https://doi.org/10.1016/S0267-7261(00)00078-6.

Ju, S.H., Liao, J.R. and Ye, Y.L. (2010), "Behavior of ground vibrations induced by trains moving on embankments with rail roughness", *Soil Dyn. Earthq. Eng.*, **30**(11), 1237-1249. https://doi.org/10.1016/j.soildyn.2010.05.006.

Kaynia, A.M., Madshus, C. and Zackrisson, P. (2000), "Ground vibration from high-speed trains: Prediction and countermeasure", *J. Geotech. Geoenviron.*, **120**(6), 531-537. https://doi.org/10.1061/(ASCE)1090-0241(2000)126:6(531).

Kouroussis, G., Van Parys, L., Conti, C. and Verlinden, O. (2014), "Using three-dimensional finite element analysis in time domain to model railway-induced ground vibrations", *Adv. Eng. Softw.*, **70**, 63-76. https://doi.org/10.1016/j.advengsoft.2014.01.005.

Kouroussis, G., Verlinden, O. and Conti, C. (2009), "Ground propagation of vibrations from railway vehicles using a finite/infinite-element model of the soil", *Proc. Inst. Mech. Eng. Part F J. Rail Rapid Transit*, **223**(4), 405-413.

Kouroussis, G., Verlinden, O. and Conti, C. (2009), "Ground propagation of vibrations from railway vehicles using a finite/infinite-element model of the soil", *Proc. Inst. Mech. Eng. Part F J. Rail Rapid Transit*, **223**(4), 405-413. https://doi.org/10.1243%2F09544097JRRT253.

Kouroussis, G., Verlinden, O. and Conti, C. (2011), "Finite-Dynamic Model for Infinite Media: Corrected Solution of Viscous Boundary Efficiency", *J. Eng. Mech.*, **137**(7), 509-511. https://doi.org/10.1061/(ASCE)EM.1943-7889.0000250.

Kouroussis, G., Verlinden, O. and Conti, C. (2011), "Free field vibrations caused by high-speed lines: measurement and time domain simulation", *Soil Dyn. Earthq. Eng.*, **31**(4), 692-707. https://doi.org/10.1016/j.soildyn.2010.11.012.

Krylov, V. (1995), "Generation of ground vibration by superfast trains", *Appl. Acoust.*, **44**(2), 149-164. https://doi.org/10.1016/0003-682X(95)91370-I.

Krylov, V. and Ferguson, C. (1994), "Calculation of low-frequency ground vibrations from railway trains", *Appl. Acoust.*, **42**(3), 199-213. https://doi.org/10.1016/0003-682X(94)90109-0.

Lefeuve-Mesgouez, G. and Mesgouez, A. (2008), "Ground vibration due to a high-speed moving harmonic rectangular load on a poroviscoelastic half-space", *Int. J. Solids Struct.*, **45**(11-12), 3353-3374. https://doi.org/10.1016/j.ijsolstr.2008.01.026.

Lefeuvemesgouez, G., Pepelow, A.T. and Lehoudec, D. (2002), "Surface vibration due to a sequence of high speed moving harmonic rectangular loads", *Soil Dyn. Earthq. Eng.*, **22**(6), 459-473. https://doi.org/10.1016/S0267-7261(02)00034-9.

Li, L., Nimbalkar, S. and Zhong, R. (2018), "Finite element model of ballasted railway with infinite boundaries considering effects of moving train loads and Rayleigh waves", *Soil Dyn. Earthq. Eng.*, **114**, 147-153. https://doi.org/10.1016/j.soildyn.2018.06.033.

Lombaert, G., Degrande, G., Kogut, J. and Francois, S. (2006), "The experimental validation of a numerical model for the prediction of railway induced vibrations", *J. Sound Vib.*, **297**(3-5), 512-535. https://doi.org/10.1016/j.jsv.2006.03.048.

Lysmer, J. and Kuhlemeyer, R.L. (1969), "Finite dynamic model for infinite media", *J. Eng. Mech. Div.*, **95**, 859-877.

Ma, L., Li, Z., Wang, M., Wei, H. and Fan, P. (2019), "Effects of size and loading rate on the mechanical properties of single coral particles", *Power Technol.*, **342**, 961-971. https://doi.org/10.1016/j.powtec.2018.10.037.

Madshus, C. and Kaynia, A.M. (2000), "High-speed railway lines on soft ground: dynamic behaviour at critical train speed", *J. Sound Vib.*, **231**(3), 689-701. https://doi.org/10.1006/jsvi.1999.2647.

Metrikine, A.V. and Popp, K. (1999), "Vibration of a periodically supported beam on an elastic half-space", *Eur. J. Mech A Solid*, **18**(4), 679-701. https://doi.org/10.1016/S0997-7538(99)00141-2.

Ren, X.W., Wu, J.F., Tang, Y.Q. and Yang, J.C. (2019), "Propagation and attenuation characteristics of the vibration in soft soil foundations induced by high-speed trains", *Soil Dyn. Earthq. Eng.*, **117**, 374-383. https://doi.org/10.1016/j.soildyn.2018.11.004.

Sheng, X., Jones, C.J.C. and Thompson, D.J. (2003), "A comparison of a theoretical model for quasi-statically and dynamically induced environmental vibration from trains with measurements", *J. Sound Vib.*, **267**(3), 621-635. https://doi.org/10.1016/S0022-460X(03)00728-4.

Sheng, X., Jones, C.J.C. and Thompson, D.J. (2006), "Prediction of ground vibration from rains using the wavenumber finite and boundary element methods", *J. Sound Vib.*, **293**(3-5), 575-586. https://doi.org/10.1016/j.jsv.2005.08.040.

Shih, J.Y., Thompson, D.J. and Zervos, A. (2016), "The effect of boundary conditions, model size and damping models in the finite element modelling of a moving load on a track/ground system", *Soil Dyn. Earthq. Eng.*, **89**, 12-27. https://doi.org/10.1016/j.soildyn.2016.07.004.

Sun, D., Yao, Y. and Matsuoka, H. (2006), "Modification of critical state models by Mohr–Coulomb criterion", *Mech. Res. Commun.*, **33**(2), 217-232. https://doi.org/10.1016/j.mechrescom.2005.05.006.

Sun, H., Cai, Y. and Xu, C. (2010), "Three-dimensional simulation of track on poroelastic half-space vibrations due to a moving point load", *Soil Dyn. Earthq. Eng.*, **30**(10), 958-967. https://doi.org/10.1016/j.soildyn.2010.04.007.

Takemiya, H. and Bian, X.C. (2005), "Substructure simulation of inhomogeneous track and layered ground dynamic interaction under train passage", *J. Eng. Mech.*, **131**(7), 699-711. https://doi.org/10.1061/(ASCE)0733-9399(2005)131:7(699).

Vostroukhov, A.V. and Metrikine, A. V. (2003), "Periodically supported beam on a visco-elastic layer as a model for dynamic analysis of a high-speed railway track", *Int. J. Solids Struct.*, **40**(21), 5723-5752. https://doi.org/10.1016/S0020-7683(03)00311-1.

Winter, M., Hyodo, M., Wu, Y., Yoshimoto, N., Hasan, M., and Matsui, K. (2017), "Influences of particle characteristic and compaction degree on the shear response of clinker ash", *Eng. Geol.*, **230**, 32-45. https://doi.org/10.1016/j.enggeo.2017.09.019.

Wu, Y., Hyodo, M. and Aramaki, N. (2018), "Undrained cyclic shear characteristics and crushing behaviour of silica sand", *Geomech. Eng.*, **14**(1), 1-8. https://doi.org/10.12989/gae.2018.14.1.001.

Wu, Y., Li, N., Hyodo, M., Gu, M., Cui, J. and Spencer, B.F. (2019), "Modeling the mechanical response of gas hydrate reservoirs in triaxial stress space", *Int. J. Hydrogen Energy*, **44**, 26698-26710. https://doi.org/10.1016/j.ijhydene.2019.08.119.

Wu, Y., Yamamoto, H. and Yao, Y. (2013), "Numerical study on bearing behavior of pile considering sand particle crushing", *Geomech. Eng.*, **5**(3), 241-261. https://dx.doi.org/10.12989/gae.2013.5.3.241.

Yao, H.L., Hu, Z., Lu, Z., Zhan, Y.X. and Liu, J. (2016), "Prediction of ground vibration from high speed trains using a vehicle–track–ground coupling model", *Int. J. Struct. Stab. Dy.*, **16**(8), 1550051. https://doi.org/10.1142/S0219455415500510.

Yaseri, A., Bazyar, M.H. and Hataf, N. (2014), "3D coupled scaled boundary finite-element/finite-element analysis of ground vibrations induced by underground train movement", *Comput. Geotech.*, **60**, 1-8. https://doi.org/10.1016/j.compgeo.2014.03.013.

Yoshimoto, N., Wu, Y., Hyodo, M. and Nakata, Y. (2016), "Effect of relative density on the shear behaviour of granulated coal ash", *Geomech. Eng.*, **10**(2), 207-224. https://doi.org/10.12989/gae.2016.10.2.207.

Zhang, R., Zhang, W., Goh, A.T.C., Hou, Z.J. and Wang, W. (2018), "A simple model for ground surface settlement induced by braced excavation subjected to a significant groundwater drawdown", *Geomech. Eng.*, **16**(6), 635-642. https://doi.org/10.12989/gae.2018.16.6.635.

CC